ODMR active bright sintered detonation nanodiamonds obtained without irradiation

© K.V. Likhachev[1,2], M.V. Uchaev[1,3], I.D. Breev[1], A.V. Ankudinov[1], R.A. Babunts[1], P.G. Baranov[1], S.V. Kidalov[1]

[1] Ioffe Institute,
194021 St. Petersburg, Russia
[2] Laboratory for diagnostics of carbon materials and spin-optical phenomena at wide-bandgap semiconductors,
Northern (Arctic) Federal University,
163002 Arkhangelsk, Russia
[3] School of Physics and Engineering, ITMO University,
197101 St. Petersburg, Russia

E-mail: kirilll281998@gmail.com

Received October 14, 2022
Revised February 18, 2023
Accepted for publication March 2, 2023

We present the results of study the structure and composition of microcrystalline diamonds obtained by high-pressure high temperature sintering of detonation nanodiamond particles. Using optical detected magnetic resonance method, photoluminescence spectroscopy and Raman spectroscopy we found sintering of detonation nanodiamond significantly differ from initial detonation nanodiamonds and can be compared to high quality diamonds. Monocrystals of diamonds obtained by the method of oriented attachment have dimensions of up to tens of microns, possess the habitus of high-quality diamonds, and do not contain metal catalysts in the lattice structure. In those crystals, the presence of optically active nitrogen impurities in the crystal lattice is observed. In particular, there is a bright nitrogen-vacancy defects. They are characterized by optical detected magnetic resonance method, which shows that spin properties of the obtained single crystals correspond to high-quality natural diamonds and surpass synthetic diamonds obtained from graphite in the presence of metal catalysts, followed by irradiation and annealing to obtain nitrogen-vacancy defects optical defects in the diamond lattice. The presence of nitrogen-vacancy defects defects and the high-quality of the crystal structure of sintering of detonation nanodiamond allows us to consider them as potential candidates in quantum magnetometry. For this purpose, the possibility of a simple way to improve the AFM probe by fixing a microcrystalline sintering of detonation nanodiamond particle on its tip is demonstrated.

Keywords: detonation nanodiamond, HPHT sintering, ODMR, single crystalline, photoluminescence, defects.

DOI: 10.21883/SC.2023.02.55954.4212

1. Introduction

Nitrogen occupies a special place in the research of diamond materials since it is the main impurity in diamond [1]. Moreover, the form in which nitrogen is contained in diamonds determines, in many respects, the properties of the latter and serves as the main factor for the classification of diamonds [2,3]. Nitrogen creates various paramagnetic centers in diamond and exists in the form of single nitrogen atoms, and in the form of nitrogen clusters [4].

Nitrogen-vacancy (NV) center in diamond (Fig. 1, *a*) is the center consisting of a nitrogen-substituted carbon atom in the diamond crystal lattice next to the missing carbon (vacancy) [5]. Two types of such centers are known: a neutral nitrogen-vacancy (NV^0) center and a negatively charged nitrogen-vacancy (NV^-) center (Fig. 1) [6]. The latter are of the greatest interest because they can be used in quantum technologies [7] and for the study of biological objects [8,9]. These staining centers can serve as biomarkers [10].

NV centers have discrete electron energy states of the intervalent zone and the diamond conduction band. The schematic of the energy levels of the NV defect is shown in Fig. 1, *b*.

The study of the optical detected magnetic resonance method (ODMR) spectra of diamonds can provide information about possible internal stresses in the crystal. Thus, it was shown in [11] that internal stresses in the diamond crystal are responsible for the increase of the spin

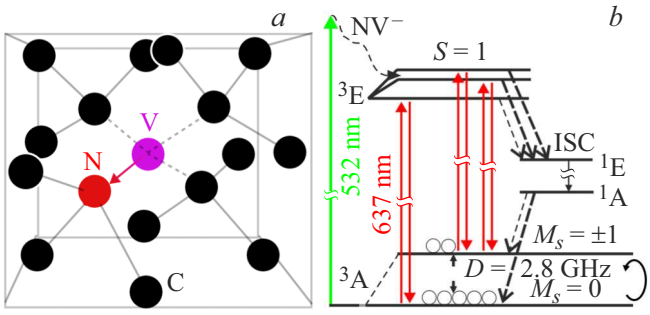

Figure 1. *a* — the diamond lattice structure, containing an NV center. *b* — diagram of the energy levels of a nitrogen — vacancy defect in diamond with optical excitation.

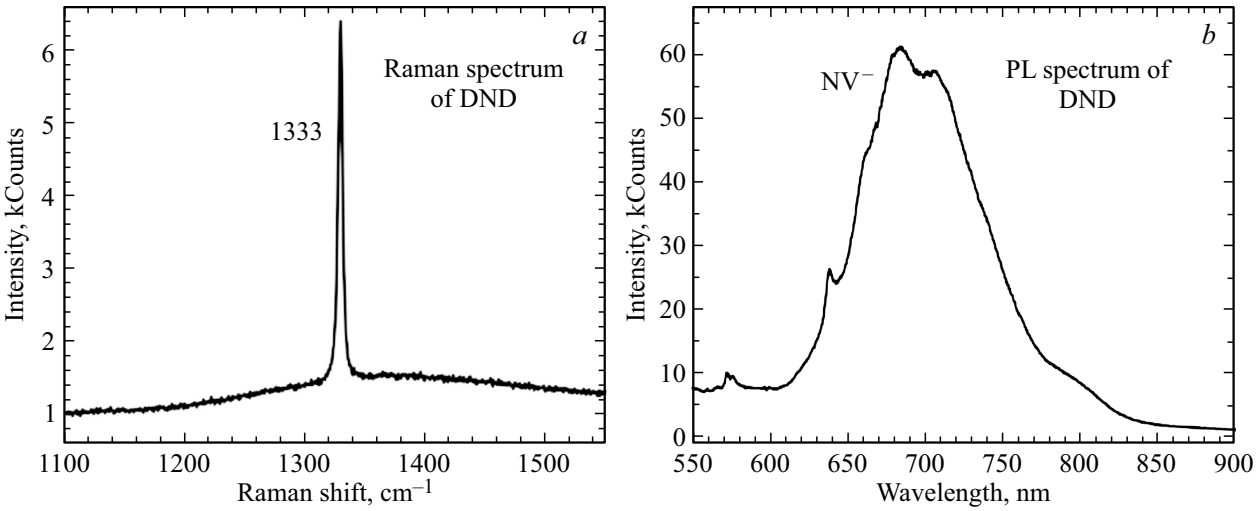

Figure 2. *a* — characteristic diamond line Raman spectrum for the obtained diamond single crystals; *b* — PL spectrum of diamond crystals at room temperature (RT) obtained from DND during HPHT sintering. Excitation at the laser wavelength of 532 nm.

Hamiltonian parameter E ($2E = 12.2 \pm 0.2$ MHz). The splitting is directly related to the stress in the crystal, and a decrease in the stresses leads to a decrease in the splitting between spin projections with $m_S = \pm 1$ (or $2E$) of the ODMR resonance line, thus making it possible to judge the crystalline perfection of diamond.

2. Experimental details

This paper investigates the ODMR spectra of diamond crystals obtained by sintering detonation diamonds at high pressures and high temperatures.

Earlier, we reported on the possibility of growth by the oriented attachment mechanism of diamond microcrystals from detonation nanodiamond (DND) nanoparticles during sintering under conditions of high pressures and high temperatures (HPHT) [12–14].

In these papers was confirmed that diamond single crystals of size between 100 nm and 15 μm are forming directly from 4–5 nm sized DND at HPHT conditions ($P \sim 7$ GPa, $T \sim 1300$–1700°C) during 8–15 s with presence of hydrocarbons (hexane) and are a white powder.

In [15,16] found by ESR method that there is distinction of composition and structure of defects in lattices of sintered microcrystals and initial DND particles.

It would be very interesting to compare the characteristics of the single crystals obtained by sintering of DND with natural diamonds and synthetic diamonds obtained by the HPHT method in the presence of metal catalysts.

Photoluminescence (PL) and Raman study was carried out at room temperature using spectrometer Sol Instruments with spectral range 200–1100 nm and resolution 0.7 nm for PL and 0.7 cm^{-1} for Raman. The excitation wavelength was 532 nm. ODMR study was carried out using hand-made setup. Optically detected magnetic resonance was measured in the 2.8–2.95 GHz region in zero magnetic fields in temperature 300 K. The ODMR spectra were recorded using standard methods: by scanning the frequency. The confocal photoluminescence acquisition system with 100x/0.9 and 100x/0.7 objective parameters was used to study nanoparticles.

For comparison, we used a high-quality type of natural diamond. The natural single crystal was irradiated with neutrons with a dose of 10^{18} cm^{-2} and annealed at a temperature of 800°C. We also used HPHT irradiated and annealed diamonds produced by Adámas Nanotechnologies (ANHPHT) with a size of 30 nm and a content of NV centers of 2–5 per particle [17] For the production of ultrasmall (as well as larger ones), nanodiamond particles containing NV centers, high-pressure high temperature (HPHT) 15–20 μm particles were irradiated with 2–3 MeV electrons to doses ranging from $5 \cdot 10^{18}$–$5 \cdot 10^{19}$ e/cm^2 followed by annealing at 850°C for 2 hrs [18].

3. Results and discussion

Using ODMR and PL spectroscopy, it was shown that such synthesized diamonds have defects of NV^0 and NV$^-$ centers in the lattice without prior irradiation with high-energy particles and subsequent annealing.

The Raman and PL study showed that with a high quality of diamond crystals, according to the Raman shift, to the corresponding natural diamond of 1333 cm^{-1} (Fig. 2, *a*), diamonds synthesized during sintering of DND have a system of optical defects in the lattice.

The Raman spectrum (Fig. 2, *a*) demonstrates the high quality of the microcrystals obtained. PL spectrum (Fig. 2, *b*) is featured by wide band of photoluminescence between 540 and 900 nm. The bright bands at 575 and 638 nm correspond to the null-phonon lines of NV^0 and NV$^-$ defects, respectively. It can be points to significant

concentration of them in diamond micro crystals sintered from DND.

For comparison with previous achievements in the field of diamond growth, we obtained the ODMR spectra of the samples of the investigated crystals of synthetic diamond HPHT with natural diamond in comparison and the ODMR spectra of diamonds obtained by sintering DND (Fig. 3).

The ODMR spectra show that the splitting of the resonance line of SDND samples is less than that of ANHPHT diamonds, and in turn is approximately equal to the splitting of the resonance in natural diamond.

The spin Hamiltonian describing NV^- centers spin system (when the quadrupole and hyperfine interaction is neglected) is

$$\mathrm{H} = g_1\mu_\mathrm{B}\mathbf{B}\cdot\mathbf{S} + D[S_Z^2 - 2/3] + E[S_X^2 - S_Y^2],$$

where μ_B is Bohr magneton, for the NV defect triplet ground state: $S = 1$, D and E represents the ZFS, e. g., $D = 2870$ MHz (for the 25°C); g factor $g_1 = 2.0028$. The parameter E is related to the deviation of the center symmetry from the axial one, which leads to splitting the 2.87 GHz ODMR line into two (Fig. 3). It should be note that the ^{14}N HF interaction for NV^- centers was not observed in these and therefore was not included in spin Hamiltonian. This indicates that the DND crystal lattice relaxes during sintering, i. e., in the sintering process the internal stresses are removed, which leads to an increase in the parameter of the spin Hamiltonian E ($2E = 12.2 \pm 0.2$ MHz) with full width at half maximum (FWHM) equal to 13.2 ± 0.2 MHz for one peak and 12.7 ± 0.2MHz for another peak. For NV centers in the natural diamond, we observe a splitting $2E = 8.8 \pm 0.1$ MHz with a FWHM equal to 5.9 ± 0.1 MHz for one peak and 6.4 ± 0.1 MHz for the other peak. For comparison, Fig. 3 also shows the ODMR spectrum of synthetic diamond

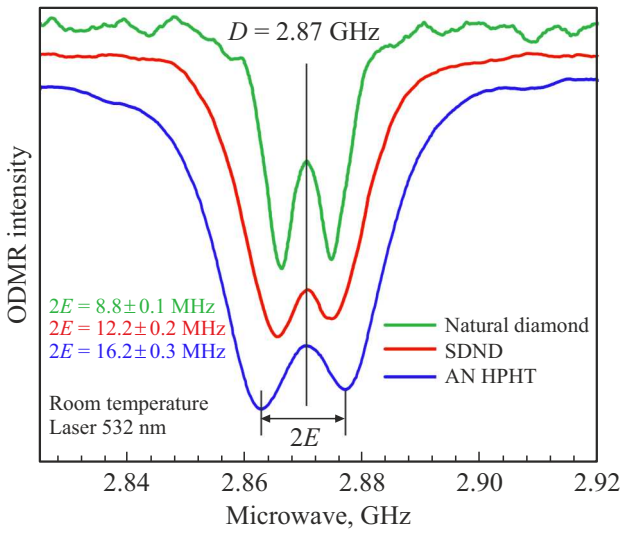

Figure 3. ODMR spectra of NV^- centers in diamond of HPHT sintered (AN HPHT), sintered DND samples (SDND) and natural diamond.

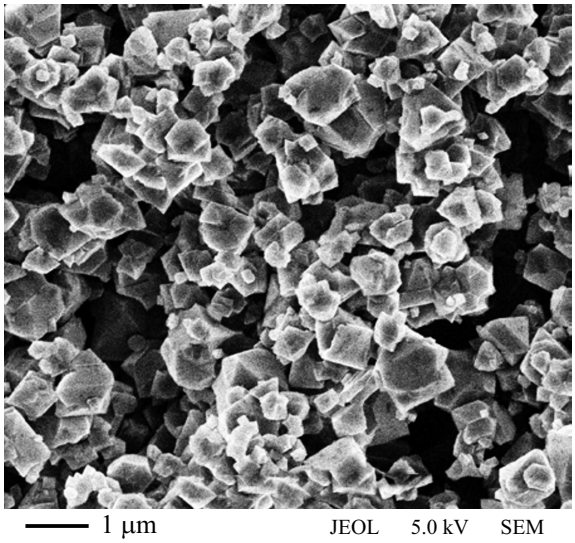

Figure 4. SEM image of microcrystals SDND. Scale bar 1 μm.

obtained under HPHT conditions. The splitting of such a sample is $2E = 16.2 \pm 0.3$ MHz with FWHM equal to 15.2 ± 0.3 MHz for one peak and 13.7 ± 0.3 MHz for the other peak.

Such facts indicate a significant transformation of the structure and composition of 4–5 nm particles of initial detonation nanodiamonds during the formation of single crystals at high pressure and high temperature.

Typical SEM images of microdiamond particles produced by HPHT sintering of DNDs is presented in Fig. 4.

In Fig. 4 it is clearly seen that diamond microcrystals are good faceted and sizes from 100 nm to units of micrometers. It is noteworthy that this type of defects was obtained without any irradiation and annealing of the single crystals obtained. Moreover, it was shown in [19] that the defective structure of microcrystalline diamonds is very different from the original detonation diamonds (DND). Thus, in contrast to the original DND, single-crystalline diamonds obtained by DND sintering do not contain nitrogen in the near-surface layers. Also, sintering of DND is accompanied by a change in their bulk electronic structure and surface chemistry, which can be seen by analyzing XAS spectra [19].

4. Nanosensors using nanodiamond

Spin defects in semiconductors are widely used for magnetic field sensing at the nanoscale. The most prominent example is the nitrogen-vacancy (NV) center in diamond, which is already being commercialized for a variety of applications, including magnetic domain imaging [20] and visualization of electrical currents [21]. The sensing principle is based on the ODMR spectroscopy. Diamond probes are usually produced using expensive and complex methods. We offer a simple way to improve a commercially available silicon AFM probe with an SDND particle.

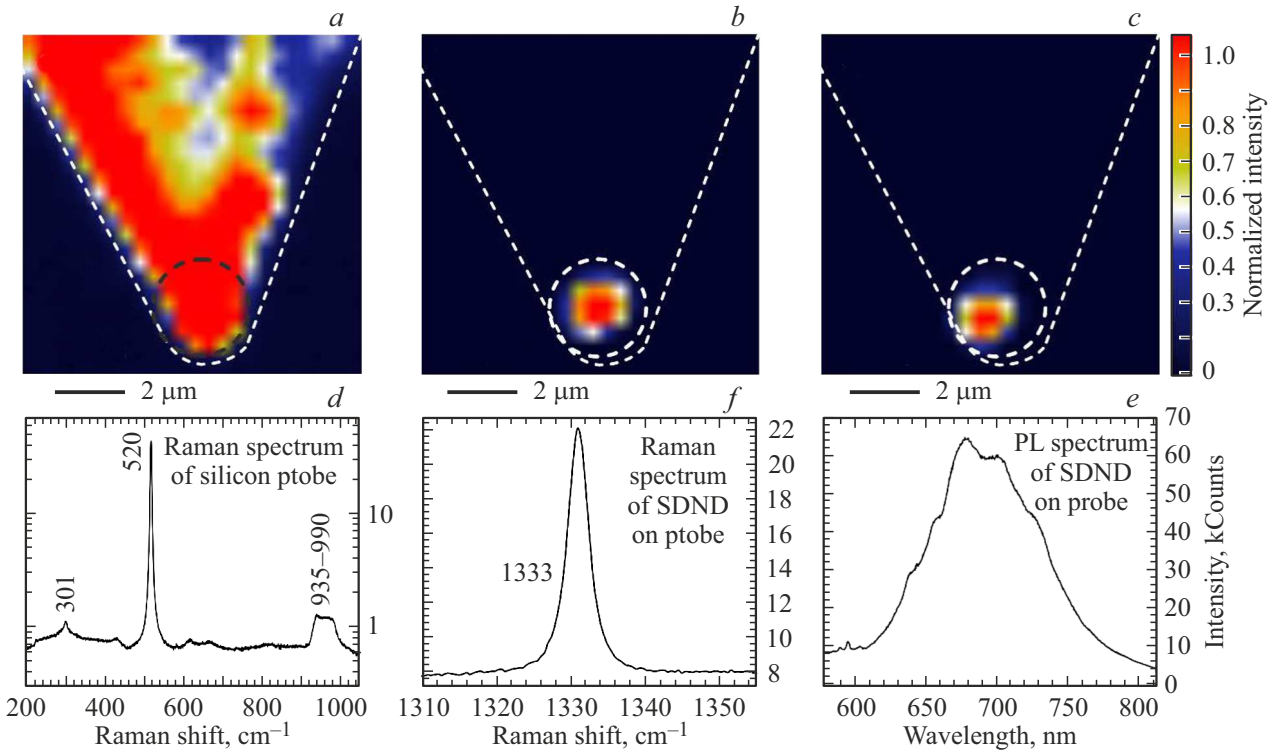

Figure 5. *a* and *b*: tone map of Raman intensity distribution from the tip of a modified silicon probe with a diamond particle. Figure, *a* — peak intensity 520 cm^{-1} (Si Raman); Figure, *b* — peak intensity 1333 cm^{-1} (Diamond Raman). The dotted circle indicates a fixed diamond particle. The height of the diamond particle chosen for the probe modification is 1.5 μm. *d* — example of Raman spectrum obtained from the brightest point of the silicon signal (520 cm^{-1}): accumulation time 150 s, pinhole 100 μm. *f* — example of Raman spectrum obtained from the brightest point of the diamond signal (1333 cm^{-1}): accumulation time 150 s, pinhole 100 μm. *c* — tone map of PL intensity distribution from the tip of a modified silicon probe with a diamond particle. *e* — example PL spectrum obtained from the brightest signal point of diamond (1333 cm^{-1}): accumulation time 10 s, pinhole 100 μm.

This method requires no additional special equipment and remains accessible to a wide range of specialists in AFM.

A UV50 urethane acrylic adhesive, which hardens when exposed to ultraviolet light, is used to fix the particle on the probe. The wetting angle α of this adhesive on the silicon substrate is about 10 degrees. The height of a spherical droplet, considering it a spherical segment of diameter d on the surface, can be obtained using the expression (1):

$$h = d\,\frac{\mathrm{tg}(\alpha/2)}{2}. \qquad (1)$$

In particular, a spherical adhesive segment with a diameter of 100 μm has a height of 4.4 μm, which is suitable for a probe with a height of 15–20 μm. The viscosity of the adhesive ($n \approx 6.5\,\mathrm{Pa}\cdot\mathrm{s}$) is such that in the semicontact or tapping AFM mode, the topography of the liquid surface of the adhesive can be visualized, and when the AFM is switched to the contact mode, the probe pierces the adhesive. The forces of viscous friction of the probe against the adhesive, estimated by Stokes formula (2), are $F_{fr} \approx 30$ nN.

$$F_{fr} = 6\pi^2 nRfa, \qquad (2)$$

where $a = 50$ nm is the vibration amplitude of the probe, the characteristic size of the adhesive contact area is approximately equal to the radius of curvature of the tip $R = 20$ nm, $f = 100$ kHz is the resonance frequency. The obtained F_{fr} is comparable to the clamping force to the solid surface calculated by formula (3)

$$F_{pr} = ka = 200\,\mathrm{nN}, \qquad (3)$$

where $k = 4$ N/m is the stiffness of the probe. The above estimates explain why it is possible in practice to scan and visualize the relief of the liquid adhesive surface in the tapping mode.

After dipping a few hundred nanometers into the glue, the tip remains „dry“, keeping the cantilever probe operable.

The following steps are performed for the manipulation. Using a probe with adhesive applied to the tip, the topography of the part of the substrate with the desired particles is scanned. Based on the obtained topography, a particle is selected for fixation, the probe is placed near the selected particle and brought into contact for a few seconds with a pressing force greater than 700 nN. The factor of the fact that the particle is fixed on the probe is its absence on the control construction of the surface relief in the semicontact mode and the increase of the characteristic sizes of the particle image. The final verification of the

fact that the particle is really fixed is made possible by obtaining Raman scattering maps of the probe tip, see Fig. 5. Figure 5 shows the analysis of the probe tip (the dotted curves — a schematic representation of the probe tip) after the SDND was fixed on it. We used the available Raman and photoluminescence spectroscopy to visualize the nanodiamond anchoring region. Excitation was performed using a 532 nm laser with a 100x objective lens with a numerical aperture of 0.7. The tone map (Fig. 5, *a* and *b*) was recorded using a confocal microscope with an aperture diameter of 100 μm in 400 nm increments and an accumulation time of 0.5 s.

The map of Raman scattering tones was obtained from a commercial silicon probe modified with an SDND particle (Fig. 5, *a*). This shows the distribution of the signal intensity from the 520 cm^{-1} line. The decrease in the intensity of this signal in the region on the right can probably be attributed to the inaccuracy of positioning and tilting of the AFM cantilever tip when scanning in the „side“ geometry. Due to the described reasons, the confocal volume, from which the signal is detected, may have different depths inside the cantilever. As the depth of focus increases, the probability of scattering of the collected Raman signal increases [22]. Therefore, the registered Raman intensity decreases as well. Fig. 5, *d* shows the spectrum obtained from the red region shown in Fig. 5, *a*. For clarity, the intensity scale is given in logarithmic values.

Similarly, AFM probes were scanned along the Raman lines (Fig. 5, *b*) and PL from NV defects (Fig. 5, *c*) in diamond. An example of the spectra obtained from the tip of the AFM probe is shown in Fig. 5, *f* and Fig. 5, *e*, respectively. The presence of the maximum intensity of both signals directly at the tip and their correspondence informs that the particle is really fixed on the AFM probe.

The ODMR spectra taken from the tip of the AFM probe with the SDND particle were studied (Fig. 6). The experiment took place at room temperature. The excitation was performed with a 532 nm laser. For comparison, an ODMR spectrum from a bulk sample (green curve) in an arbitrary orientation is also presented.

In an external magnetic field of 70 G there is a splitting into 4 lines, corresponding to the orientation of the four NV center axes in the diamond. According to the positions of the peaks, it is possible to estimate the values of all magnetic field projections using [23]:

$$f_{\pm}(\bar{B}) = D + \frac{3\gamma_e^2 B^2}{2D} \sin^2\theta_B \pm \gamma_e B \times \cos\theta_B \sqrt{1 + \frac{\gamma_e^2 B^2}{4D^2} \operatorname{tg}^2\theta_B \sin^2\theta_B}, \quad (4)$$

where $B = \sqrt{B_z^2 + B_\perp^2}$, $B_\perp = \sqrt{B_x^2 + B_y^2}$, $\operatorname{tg}\theta_B = \frac{B_\perp}{B_z}$, $\gamma_e = \frac{g_e \mu_B}{\hbar}$, $g_e \sim 2.003$ — g-factor of electron, μ_B — Bohr magneton, the z-axis is directed along the major symmetry axis of the NV^- center. And by the maximum distance between the peaks (the leftmost ~ 2.68 GHz and the rightmost ~ 3.05 GHz) you can estimate the size of the external magnetic field.

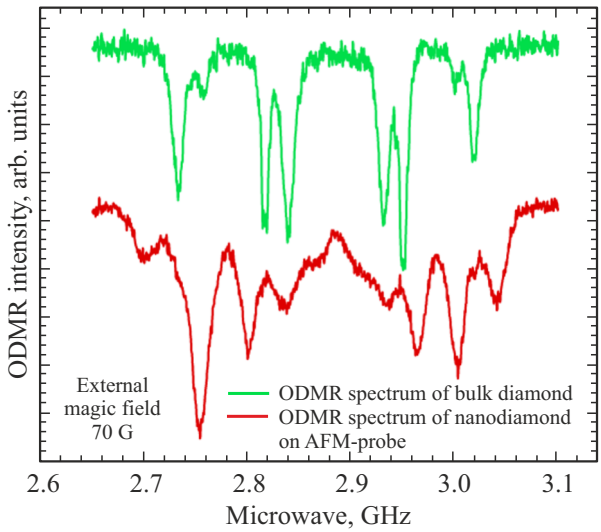

Figure 6. ODMR spectrum of bulk diamond (green curve) and nanodiamond SDND on AFM-probe (red curve). The spectrum was taken in an external magnetic field of 70 Gauss. laser excitation 532 nm. You can see the splitting into 4 lines (on one side of the 2.88 GHz center), which correspond to the four orientations of the NV^- center axes.

5. Conclusions

Thus, HPHT sintering of 4–5 nm DND particles provides effective formation of 0.1–15 μm sized high quality single crystal diamonds with bulk electronic structure and structural perfection very similar the ones of macroscopic high quality single crystal diamonds.

That sintering of DND 4–5 nm particles at HPHT condition results in transformation of their PL spectra to the shape inherent to the perfect crystalline diamond with noticeable content of luminescent NV^- centers.

ODMR study demonstrate, that the splitting of the resonance line of sintered SDND samples is smaller than that of HPHT diamond and approximately equal to the splitting of the resonance in natural diamond single crystal. Thus, we showed that the quality of synthesized diamonds with NV defects is higher than the quality of diamonds previously obtained by other methods.

Acknowledgments

The research was carried out in the frame of the Government Topical Program for Ioffe Institute (project 0040-2014-0013 „Physical-chemical basics of technology for new functional materials based on carbon nanostructures“). The research was partly supported by the state task of the Russian Federation N FSRU-2021-0008. The research AFM with nanodiamond supported under the „ERA.Net

RUS plus“ program and funded by RFBR, project number 20-52-76010.

Conflict of interest

The authors declare that they have no conflict of interest.

References

[1] H. Kanda, M. Akaishi, S. Yamaoka, Y. Shinobu. Diamond. Relat. Mater., **8** (8–9), 1441 (1999).
[2] H. Sumiya, N. Toda, S. Satoh. SEI Tech. Rev., **60**, 10 (2005).
[3] H. Sumiya, S. Satoh. Diamond. Relat. Mater., **5** (11), 1359 (1996).
[4] R. Schirhagl, K. Chang, M. Loretz, C.L. Degen. Ann. Rev. Phys. Chem., **65**, 83 (2014).
[5] C. Bradac, T. Gaebel, J.R. Rabeau. Optical Engin. Diamond., 143 (2013).
[6] L. Rondin, G. Dantelle, A. Slablab, F. Grosshans, F. Treussart, P. Bergonzo, S. Perruchas, T. Gacoin, M. Chaigneau, H.-C. Chang, V. Jacques, J.-F. Roch. Phys. Rev. B, **82**, 115449 (2010).
[7] F. Kong, C. Ju, Y. Liu, C. Lei, M. Wang, X. Kong, P. Wang, P. Huang, Z. Li, F. Shi, L. Jiang, J. Du. Phys. Rev. Lett., **117**, 060503 (2016).
[8] T. Zhang, G. Pramanik, K. Zhang, M. Gulka, L. Wang, J. Jing, F. Xu, Z. Li, Q. Wei, P. Cigler, Z. Chu. ACS Sens., **6** (6), 2077 (2021).
[9] F. Morales-Zavala, N. Casanova-Morales, R.B. Gonzalez, A. Chandía-Cristi, L.D. Estrada, I. Alvizú, V. Waselowski, F. Guzman, S. Guerrero, M. Oyarzún-Olave, C. Rebolledo, E. Rodriguez, J. Armijo, H. Bhuyan, M. Favre, A.R. Alvarez, M.J. Kogan, J.R. Maze. J. Nanobiotechnology, **16** (1), 1 (2018).
[10] L.J. Rogers, M.W. Doherty, M.S. Barson, S. Onoda, T. Ohshima, N.B. Manson. New J. Phys., **17** (1), 013048 (2015).
[11] S.V. Kidalov, F.M. Shakhov, A.Ya. Vul', A.N. Ozerin. Diamond. Relat. Mater., **19** (7–9), 976 (2010).
[12] S.V. Kidalov, F.M. Shakhov, A.V. Shvidchenko, A.N. Smirnov, V.V. Sokolov, M.A. Yagovkina, A. Ya. Vul'. Techn. Phys. Lett., **43** (1), 53 (2017).
[13] A.T. Dideikin, E.D. Eidelman, S.V. Kidalov, D.A. Kirilenko, A.P. Meilakhs, F.M. Shakhov, A.V. Shvidchenko, V.V. Sokolov, R.A. Babunz, A.Ya. Vul'. Diamond. Relat. Mater., **75**, 85 (2017).
[14] A.A. Soltamova, I.V. Ilyin, P.G. Baranov, A.Ya. Vul', S.V. Kidalov, F.M. Shakhov, G.V. Mamin, S.B. Orlinskii, N.I. Silkin, M.Kh. Salakhov. Phys. B: Condens. Matter., **404** (23–24), 4518 (2009).
[15] V.Yu. Osipov, F.M. Shakhov, N.N. Efimov, V.V. Minin, S.V. Kidalov, A.Ya. Vul'. Phys. Solid State, **59**, 1146 (2017).
[16] Adámas Nanotechnologies, Inc, NV- High Brightness Series: Product Sheet, **9** (8/18), 1 (2018). [Online]. Available: https://www.adamasnano.com/wp-content/uploads/2019/02/NV-High-Brightness-Series-Product-Sheet.pdf
[17] O. Shenderova, N. Nunn, T. Oeckinghaus, M. Torelli, G. McGuire, K. Smith, E. Danilov, R. Reuter, J. Wrachtrup, A. Shames, D. Filonova, A. Kinev. Adv. Phot. Quant. Computing, Memory, and Commun., **10118**, 2 (2017).
[18] S.V. Kidalov, V.V. Shnitov, M.V. Baidakova, M. Brzhezinskaya, A.T. Dideikin, M.S. Shestakov, D.A. Smirnov, I.T. Serenkov, V.I. Sakharov, V.V. Sokolov, N.I. Tatarnikov, A. Ya. Vul. Nanosystems: physics, chemistry, mathematics, **9** (1), 21 (2018).
[19] Q.C. Sun, T. Song, E. Anderson, A. Brunner, J. Förster, T. Shalomayeva, T. Taniguchi, K. Watanabe, J. Gräfe, R. Stöhr, X. Xu, J. Wrachtrup. Nature Commun., **12** (1), 1989 (2021).
[20] R. Dou, G. Zhu, W.H. Leong, X. Feng, Z. Li, C. Lin, S. Wang, Q. Li. Carbon, **203**, 534 (2023).
[21] F. Adar, E. Lee, S. Mamedov, A. Whitley. Microscopy and Microanalysis, **16** (S2), 360 (2010).
[22] M.W. Doherty, J. Michl, F. Dolde, I. Jakobi, P. Neumann, N.B. Manson, J. Wrachtrup. New J. Phys., **16** (6), 063067 (2014).